Optoelectronics and optoelectronic devices

Influence of the thickness of frontal platinum metallic layer on the electro-optical characteristics of GaN-based Schottky ultraviolet photodetectors

F. Bouzid[1,*], F. Pezzimenti[2]

[1]*Research Center in Industrial Technologies CRTI, P.O. Box 64, Cheraga, 16014 Algiers, Algeria*
[2]*DIIES-Mediterranea University of Reggio Calabria, Reggio Calabria 89122, Italy*
[*]*Corresponding author email: f.bouzid@crti.dz*

Abstract. In this work, we evaluated the effect of the thickness of frontal metallic layer on the electro-optical characteristics of an *n*-type gallium nitride (*n*-GaN)-based Schottky barrier ultraviolet (UV) detector using device modeling and numerical simulations. Comparison of the current density-voltage characteristics $J(V)$ calculated for different metals demonstrated that platinum (Pt) is the most suitable metal to form Schottky contacts. The obtained results show that the thickness of the frontal platinum Schottky contact highly affects the spectral responsivity of the detector in the considered UV range of 0.2…0.4 µm. In particular, the detector responsivity at room temperature can reach the peak value of 0.208 $A \cdot W^{-1}$ at the wavelength of 0.364 µm and the semi-transparent Pt layer as thin as 1 nm. Afterward, it gradually decreases with the increase of the metal layer thickness down to 0.147 $A \cdot W^{-1}$ for the thickness of the Pt layer of 100 nm.

Keywords: gallium nitride, Schottky barrier, ultraviolet detector, photocurrent, responsivity.

https://doi.org/10.15407/spqeo25.03.323
PACS 73.30.-y, 73.61.Ey, 85.60.Bt, 85.60.-q

Manuscript received 17.03.22; revised version received 05.08.22; accepted for publication 21.09.22; published online 06.10.22.

1. Introduction

Large bandgap materials have been widely studied recently due to their potential applications in field effect transistors (FET), high power electronics, nuclear micro-batteries, laser devices, light emitting diodes (LED), and ultraviolet (UV) photodetectors [1–11]. Among these materials, gallium nitride (GaN) stands out as a promising compound that offers great performance improvements in harsh environments, meeting essential requirements such as high breakdown electric fields and good transport properties. In particular, detection of UV radiation with GaN-based devices has attracted large interest for many applications requiring high-performance solar-blind detectors with high responsivity. Accordingly, various device structures (*e.g.*, *p-n*, *p-i-n*, metal/semiconductor, metal/semiconductor/metal, *etc.*) have been investigated [12–17].

For several years, GaN-based Schottky barrier UV photodetectors have been studied by numerous researchers. Referring to the literature, we can cite the work by Q. Chen *et al.* [18] reporting a Schottky barrier UV photodetector (Pd/*n*-GaN), which provides the maximum spectral response of 0.18 $A \cdot W^{-1}$ at 365 nm under the 5 V reverse polarization. This detector consists of a 1-µm thick GaN layer with the donor doping concentration of $3 \cdot 10^{18}$ cm^{-3} deposited on a sapphire substrate and an active *n*-GaN layer (0.4 µm, $3 \cdot 10^{16}$ cm^{-3}). D.G. Zhao and D.S. Jiang [19] reported photodetectors (Ni/Au/n-GaN) which had the maximum spectral response of 0.2 $A \cdot W^{-1}$ at 365 nm under zero voltage polarization. S. Zhang *et al.* [20] designed a Schottky barrier UV photodetector which showed the peak of spectral response exceeding 0.15 $A \cdot W^{-1}$ at 258 nm under zero voltage polarization. This detector consists of a 0.4-µm thick unintentionally doped ($1.6 \cdot 10^{16}$ cm^{-3}) active layer (*n*-GaN), a 4-µm thick heavily doped ($3 \cdot 10^{18}$ cm^{-3}) layer (n^+-GaN), and a semi-transparent Ni/Au multilayer acting as the Schottky contact. W. Mou *et al.* [21] reported a high performance UV photodetector having the spectral response peak equal to 0.147 $A \cdot W^{-1}$ at 360 nm under zero voltage polarization. Finally, we can cite the work by X. Sun *et al.* [22], where the authors presented alternative GaN-based UV photodetectors with the Schottky contacts in the form of inter-penetrating fingers of Ni/GaN/Cr, Ni/GaN/Ag, and Ni/GaN/Ti/Al. These photodetectors have demonstrated the spectral responses of approximately 0.037, 0.083, and 0.104 $A \cdot W^{-1}$, respectively, under zero polarization condition.

© 2022, V. Lashkaryov Institute of Semiconductor Physics, National Academy of Sciences of Ukraine

It is important to note that all the mentioned works were carried out after overcoming many crucial technological issues, the most prominent of which was obtaining an effective metallic contact to GaN. However, the published works on Schottky barrier photodetectors usually do not provide explanations concerning the influence of the thickness of metallic layer, which is used to create Schottky barrier, on the electro-optical characteristics of device.

In this context, the main purpose of this work is to simulate the current density-voltage $J(V)$ characteristics as well as the spectral response $SR(\lambda)$ of a GaN-based UV detector at room temperature. The Schottky contact consists of a semi-transparent platinum layer. the detector spectral responsivity was found to exceed 0.2 $A\cdot W^{-1}$ at zero bias voltage. The presented results have been obtained by simulations using the SILVACO Atlas technology computer-aided design (TCAD) simulator. In particular, we have estimated the leakage current values in the structures consisting of an *n*-type GaN layer and a single layer Schottky contact made of the following metals: platinum (Pt), nickel (Ni), gold (Au), silver (Ag), chromium (Cr), and molybdenum (Mo). Platinum has been chosen for fabrication of Shottky contacts as providing the lowest leakage current value. The paper also presents an evaluation study of the effect of the thickness of semi-transparent metallic layer on the fundamental photodetector properties. The simulated current density has been obtained by varying the direct polarization voltage between 0 and 3.2 V and reverse one between –300 V and 0 V. The spectral responsivity has been calculated within the UV spectral range of 0.2 to 0.4 μm.

The investigated structure consisted of a 5-μm-thick *n*-GaN epitaxial layer with the donor atom concentration of $1\cdot10^{16}$ cm^{-3} deposited on n^+-GaN substrate with the doping concentration of $5\cdot10^{19}$ cm^{-3}. We started our study by assuming that the anode thickness is 1 nm (metallic layer) and the density of states at the interface between the metal and the active region equals to $1\cdot10^{6}$ cm^{-3}. Finally, an ohmic contact of titanium-aluminum alloy (TiAl) over the entire rear surface was considered. The total area of the device surface was 12 μm^2. A 2-D rectangular mesh over the device structure, which was precisely refined at the metal/*n*-GaN and *n*-GaN/n^+-GaN interfaces, was used in the simulations.

2. Physical models

The key physical models used in the simulations include the Shockley–Read–Hall (SRH) and the Auger recombination processes, the incomplete doping activation, the impact ionization, the temperature dependence of the bandgap value, and the carrier mobility as a function of both doping and temperature. The temperature dependences of the GaN bandgap [23] and the intrinsic carrier concentration [24] are assumed to have the following forms:

$$E_g(T) = E_{g0} + 9.39\cdot10^{-4}\left(\frac{300^2}{300+772} - \frac{T^2}{T+772}\right), \quad (1)$$

$$n_i(T) = 1.98\cdot10^{16}\cdot T^{3/2}\exp\left(-\frac{20488}{T}\right), \quad (2)$$

where E_{g0}= 3.396 eV is the bandgap energy at T = 300 K.

Starting from the effective intrinsic carrier concentration, the rates of the Auger and SRH recombination as well as the optical generation-recombination process are described by the standard expressions [25, 26]:

$$R_{\mathrm{Auger}} = \left(C_p p + C_n n\right)\left(np - n_i^2\right), \quad (3)$$

$$R_{\mathrm{SRH}} = \frac{pn - n_i^2}{\tau_p\left(n + n_i\exp\left(\frac{E_{trap}}{kT}\right)\right) + \tau_p\left(p + n_i\exp\left(-\frac{E_{trap}}{kT}\right)\right)}, \quad (4)$$

$$R_{opt} = C_{opt}\left(np - n_i^2\right), \quad (5)$$

where C_n = $1\cdot10^{-30}$ $cm^6\cdot s^{-1}$, C_p = $1\cdot10^{-31}$ $cm^6\cdot s^{-1}$ and C_{opt} = $1.1\cdot10^{-8}$ $cm^3\cdot s^{-1}$ are the model coefficients, E_{trap} is the difference between the trap energy level and the intrinsic Fermi level, and τ_n and τ_p are the carrier lifetimes, which depend on the doping level, as described by Scharfetter's relation [25]:

$$\tau_{n,p} = \frac{\tau_{0n,p}}{1 + \left(\frac{N}{N_{n,p}^{\mathrm{SRH}}}\right)^{\gamma_{n,p}}}. \quad (6)$$

Here, N is the total impurity concentration in a given device region, $\tau_{0n,p}$ = 0.5 ns, $N_{n,p}^{\mathrm{SRH}} = 5\cdot10^{16}\,\mathrm{cm^{-3}}$, and γ = 1 [24].

The dependence of the rate of charge carrier photogeneration on the incident beam wavelength is given by [27]:

$$G = \eta_0\frac{P^*\lambda}{hc}\alpha e^{-\alpha y}, \quad (7)$$

where P^* contains the cumulative effects of reflections, transmissions and losses due to the absorption over the beam path, η_0 is the internal quantum efficiency, which represents the number of carrier pairs generated per photon, y is the relative distance passed by the beam under consideration, h is the Planck's constant, λ is the wavelength, c is the speed of light, and α is the absorption coefficient, respectively.

The electron and hole impact ionization rates, $\alpha_{n,p}$, which are defined as the numbers of electron-hole pairs generated by the carriers traveling a unit distance along the direction of the electric field, are calculated using the following empirical expression:

$$\alpha_{n,p} = a_{0n,p}\exp\left(-\frac{b_{0n,p}}{E}\right), \quad (8)$$

where the used coefficients a_0 and b_0 are listed in Table 1.

Table 1. GaN impact ionization parameters.

Carrier	a_0, cm^{-1}	b_0, V·cm^{-1}
electron	$2.41\cdot10^8$	$3.40\cdot10^7$
hole	$5.41\cdot10^6$	$1.96\cdot10^7$

Assuming the Fermi–Dirac statistics, the incomplete ionization of impurities can be described by the following expressions [28]:

$$N_d^+ = \frac{N_d}{1+2\left(\frac{N_d}{N_C}\right)\exp\left(\frac{\Delta E_d}{kT}\right)}, \quad (9)$$

$$N_a^+ = \frac{N_a}{1+4\left(\frac{N_a}{N_V}\right)\exp\left(\frac{\Delta E_a}{kT}\right)}, \quad (10)$$

where N_d and N_a are the concentrations of substitutional n- and p-type dopants, ΔE_a and ΔE_d are the acceptor and donor energy levels (*e.g.*, ΔE_d = 16 meV for Si and ΔE_a = 175 meV for Mg), and N_C and N_V are the electron and hole densities of states varying with temperature, as given in Ref. [24]:

$$N_C(T) = 2.3\cdot10^{18}\left(\frac{T}{300}\right)^{3/2}, \quad (11)$$

$$N_V(T) = 4.6\cdot10^{19}\left(\frac{T}{300}\right)^{3/2}. \quad (12)$$

Finally, the Caughey–Thomas analytic model [29] is used to calculate the carrier mobilities:

$$\mu_{n,p} = \mu_{\max n,p} + \frac{\mu_{\max n,p}\left(\frac{T}{300}\right)^{\alpha} - \mu_{\min n,p}}{1+\left(\frac{T}{300}\right)^{\beta}\left(\frac{N_{tot}}{N_{ref}}\right)^{\gamma}}. \quad (13)$$

Here, N_{tot} is the local (total) concentration of the ionized impurities, and $\mu_{\min n,p}$, $\mu_{\max n,p}$, α, β, and γ are the GaN-specific model parameters listed in Table 2 [30].

In addition, the Canali model [31] is used to calculate the high field-dependent mobility:

$$\mu_{n,p}(E) = \mu_{0n,p}\left[1+\left(E\frac{\mu_{0n,p}}{v_{sat}}\right)^{\kappa_{n,p}}\right]^{-1/\kappa_{n,p}}, \quad (14)$$

where $\mu_{0n,p}$ is the low electric field mobility and v_{sat} is the temperature-dependent saturation velocity given in Ref. [26]:

$$v_{sat} = \frac{2.7\cdot10^7}{1+0.8\exp\left(\frac{T}{600}\right)}. \quad (15)$$

Table 2. GaN carrier mobility parameters.

Carrier	μ_{max}, cm²/V·s	μ_{min}, cm²/V·s	N_{ref}, cm^{-3}	α	β	γ
electron	1418	55	$2\cdot10^{17}$	–2	–3.8	1
hole	175	30	$3\cdot10^{17}$	–5	–3.7	2

3. Results and discussion

3.1. *J*(*V*) characteristics for different metal/*n*-GaN structures

Fig. 1 shows the *J*(*V*) characteristics of the contacts between the *n*-GaN layer and different metals, namely Pt, Ni, Au, Ag, Cr, and Mo, whose adopted output work functions were 5.65, 5.15, 5.1, 4.81, 4.5, and 4.3 eV, respectively [32–35]. These characteristics are plotted on a logarithmic scale to emphasize their exponential behavior.

It is worth mentioning that the typical *J*(*V*) characteristic in dark for the studied *n*-GaN UV Schottky barrier detector with Pt contact is well-plotted. It can be seen from Fig. 1a that thanks to the higher metal work function, this characteristic shows high non-linearity and

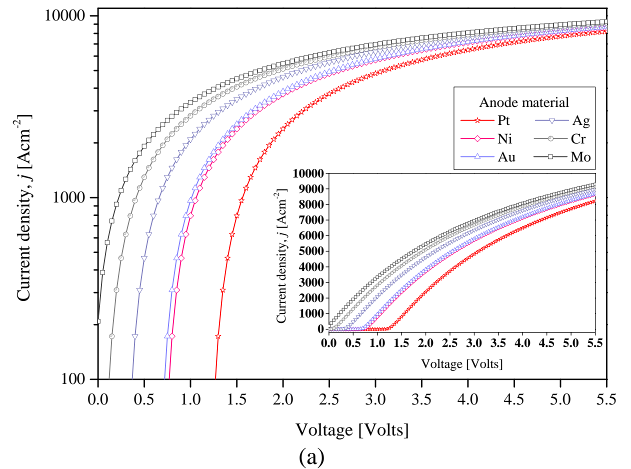

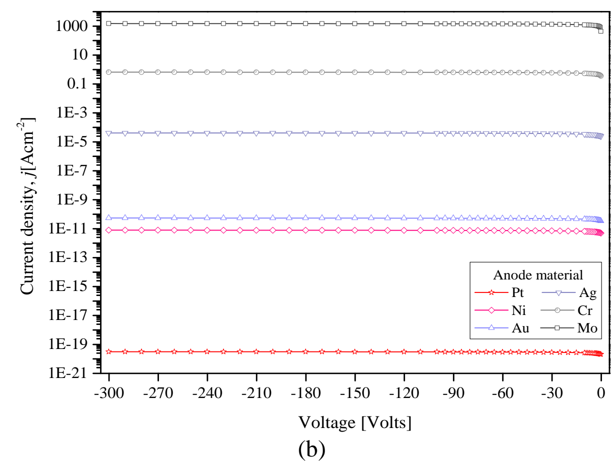

Fig. 1. *J*(*V*) characteristics of the contact between the *n*-GaN layer and the Pt, Ni, Au, Ag, Cr, and Mo metal. (a) forward polarization, (b) reverse polarization.

strong rectification behavior with the turn-on voltage close to 1.3 V, which is the highest value as compared to other metal contacts.

On the other hand, by comparing the $J(V)$ characteristics in Fig. 1b, obtained for different metals under reverse polarization, we found that Pt ensures the lowest leakage current. From these results, Pt appears as the best candidate for fabrication of high quality Schottky contacts on *n*-GaN substrates.

3.2. Analysis of the anode thickness effect

3.2.1. *J*(*V*) characteristics in dark

Simulating the device $J(V)$ characteristics in dark in accordance with the thermionic emission theory, a very limited effect of the thickness of Pt layer was noticed. In particular, the thickness was varied in the range of 0.1 to 100 nm and both forward and reverse bias conditions were considered. The obtained results are reported in Fig. 2.

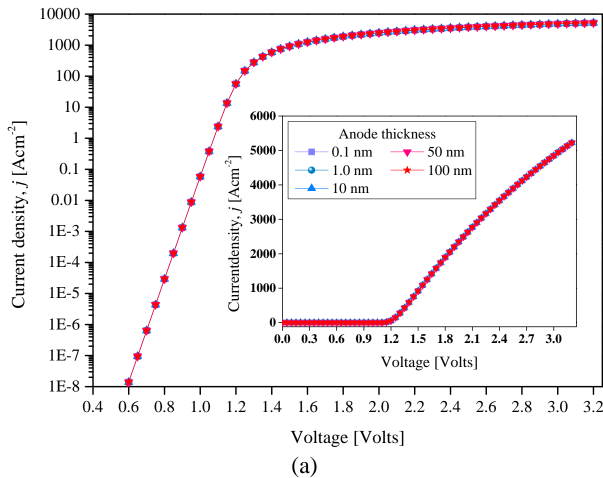

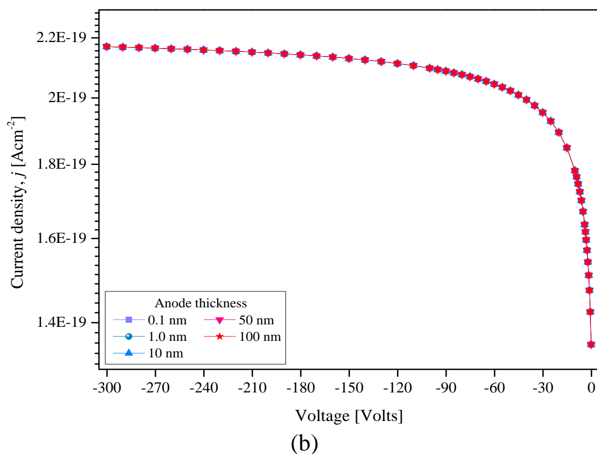

Fig. 2. $J(V)$ characteristics in dark for the UV radiation detector (Pt/*n*-GaN) with different anode thicknesses at T = 300 K. (a) forward polarization (inset: $J(V)$ characteristics in linear scale), (b) reverse polarization.

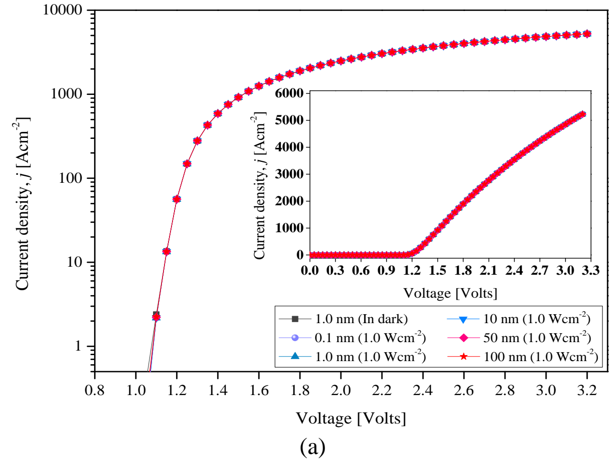

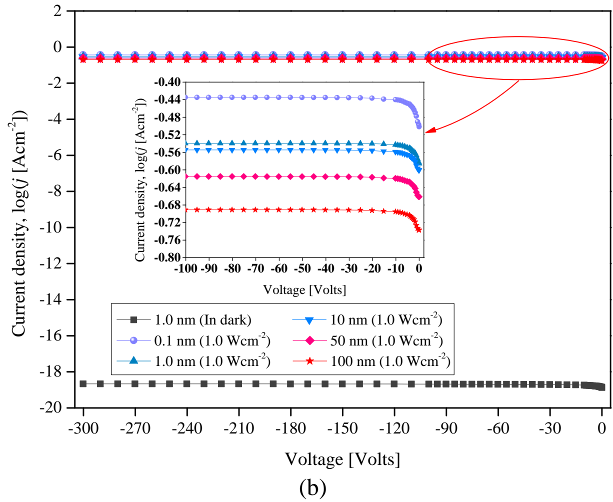

Fig. 3. $J(V)$ characteristics of the (Pt/*n*-GaN) detector for different anode thicknesses under 1 W·cm^{-2} illumination intensity with λ = 0.36 µm. (a) forward polarization (inset: $J(V)$ characteristics in linear scale), (b) reverse polarization (inset: zoom-in of the circled area).

3.2.2. *J*(*V*) characteristics under illumination

Fig. 3 shows the $J(V)$ curves under illumination for the Pt/*n*-GaN detector with different anode thicknesses at the beam intensity of 1 W·cm^{-2} and the UV radiation wavelength of 0.36 µm.

From Fig. 3a, we can note a very small effect of the anode thickness on the $J(V)$ characteristics under forward bias condition. In particular, the quantity of photons which move towards the *n*-GaN layer due to absorption remains almost unchanged with the increase of the anode thickness. This result is consistent with the limited variations of the photogeneration rate along the device plotted in Fig. 4. As also follows from Fig. 4, the obtained values of the photogeneration rate are always rather low.

In particular, we can state that forward bias induces rapid recombination of photo-generated carriers due to the weak electric field and the reduction of the width of depletion region. Therefore, it appears that the detector

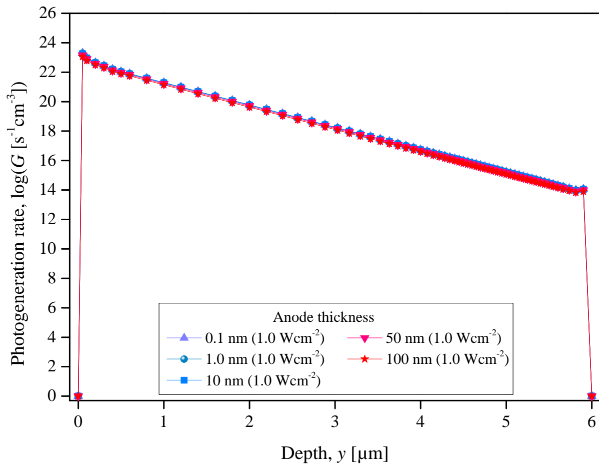

Fig. 4. Photogeneration rate profiles for different anode thicknesses under the UV illumination with the intensity of 1.0 W·cm^{-2} and λ = 0.36 μm.

(a)

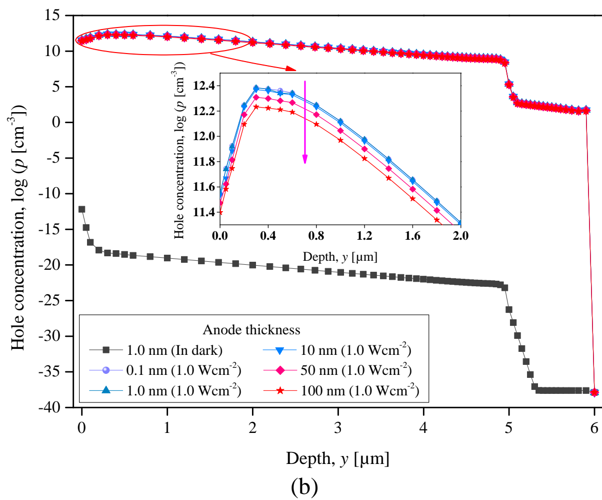

(b)

Fig. 5. Charge carrier concentration profiles under forward bias condition (1.3 V) for different anode thicknesses. The device is under the UV illumination with the intensity of 1 W·cm^{-2} and λ = 0.36 μm. (a) electrons, (b) holes.

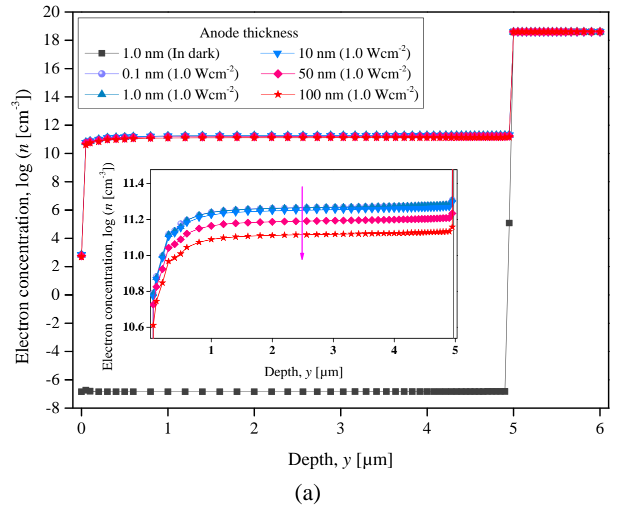

(a)

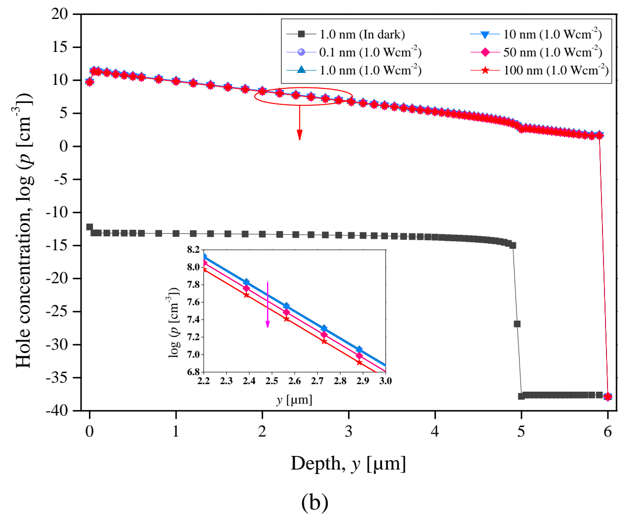

(b)

Fig. 6. Charge carrier concentration profiles under reverse bias condition (–300 V) for different anode thicknesses. The device is under the UV illumination with the intensity of 1 W·cm^{-2} and λ = 0.36 μm. (a) electrons, (b) holes.

does not respond to illumination. This conclusion can be confirmed by the charge carrier concentration profiles in the device at the forward bias of 1.3 V plotted in Fig. 5. It is evident from this figure that the electron and hole concentration profiles show a very limited decrease with the increase of the anode thickness.

On the other hand, Fig. 3b clearly shows the effect of the anode thickness on the $J(V)$ characteristics under reverse bias condition. At this, the current density decreases with increasing the anode thickness. This is due to the decrease in the photogeneration rate caused by the reduction in the amount of photons that reach the n-GaN active region. Obviously, this result is caused by the different absorption defined by the metallic layer. The charge carrier concentration profiles in the detector plotted at a reverse bias equal to –300 V are shown in Fig. 6.

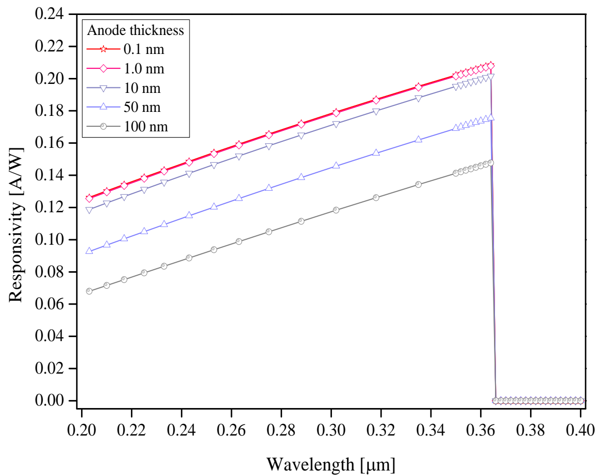

Fig. 7. Spectral responsivity of the Schottky detector (Pt/*n*-GaN) for different anode thicknesses at the radiation intensity of 1 W·cm^{-2} and zero bias voltage.

3.2.3. Spectral responsivity

The spectral responsivity of a photodiode determines the efficiency of converting illumination power into electric current. To evaluate the influence of the thickness of the frontal platinum contact on the spectral responsivity of the proposed device, we have simulated the spectral responsivity as a function of the incident radiation wavelength at five different thicknesses of the frontal contact layer (*i.e*., 0.1, 1.0, 10, 50, and 100 nm). In the simulations, we used the UV radiation spectrum in the wavelengths range of 0.2 to 0.4 μm and the radiation intensity of 1 W·cm^{-2}. The obtained results are shown in Fig. 7.

According to the results presented in Fig. 7, we can state that increasing the radiation wavelength from 0.2 to 0.364 μm leads to progressive rise of the spectral responsivity from 0.126 up to 0.208 A·W^{-1} with subsequent sharp drop at the cutoff wavelength of 364 nm in the case of the semi-transparent metallic layer (0.1…1.0 nm). However, at the thicknesses higher than 10 nm, a significant reduction in the charge carriers photogeneration is observed. At this, the responsivity peak tends to decrease gradually down to 0.147 A·W^{-1} for the Pt thickness of 100 nm.

Thicker anode means longer path for photons and charge carriers. As a result, a significant portion of UV radiation energy is lost the detector has higher polarization resistance and its performance is reduced.

4. Conclusions

In this paper, an electro-optical study of a GaN-based Schottky barrier UV-detector is presented focusing on the influence of the Schottky contact thickness on the detector electro-optical characteristics.

It was found from the simulation results that the *J*(*V*) characteristics in the case of platinum have the highest non-linearity and rectification behavior, the turn-on voltage close to 1.3 V as well as the lowest leakage current as compared to the other explored metal contacts. These results are attributed to the high work function of Pt.

On the other hand, the obtained results show that increase in the thickness of the platinum metallic layer above 10 nm leads to the enhancement of the degradation of detector efficiency when the detector is illuminated with UV radiation with the wavelength of 0.36 μm and the beam intensity of 1 W·cm^{-2}. Moreover, at zero bias voltage, *T* = 300 K and under the same irradiation conditions as in the previous case, the detector responsivity, which reaches the peak value of 0.208 A·W^{-1} at the wavelength of 0.364 μm for the semi-transparent platinum metallic layer (~1 nm), decreases to 0.147 A·W^{-1} at the Pt thickness of 100 nm. Such a behavior was explained by significant loss of UV radiation energy by absorption as well as the high polarization resistance phenomenon.

References

1. Whiteside M., Arulkumaran S., Ng G.I. Demonstration of vertically-ordered h-BN/AlGaN/GaN metal-insulator-semiconductor high-electron-mobility transistors on Si substrate. *Mater. Sci. Eng.: B*. 2021. **270**. P. 115224. https://doi.org/10.1016/j.mseb.2021.115224.
2. Bergamim L.F.O., Parvais B., Simoen E., de Andrade M.G.C. Analog performance of GaN/AlGaN high-electron-mobility transistors. *Solid-State Electronics*. 2021. **183**. P. 108048. https://doi.org/10.1016/j.sse.2021.108048.
3. Bouzid F., Saeed M.A., Carotenuto R., Pezzimenti F. Design considerations on 4H-SiC-based *p-n* junction betavoltaic cells. *Appl. Phys. A*. 2022. **128**. P. 234. https://doi.org/10.1007/s00339-022-05374-7.
4. Bouzid F., Pezzimenti F., Dehimi L. Modelling and performance analysis of a GaN-based *n/p* junction betavoltaic cell. *Nucl. Instrum. Methods Phys. Res. Section A*. 2020. **969**. P. 164103. https://doi.org/10.1016/j.nima.2020.164103.
5. Bouzid F., Dehimi S., Hadjab M. *et al.* Performance prediction of AlGaAs/GaAs betavoltaic cells irradiated by nickel-63 radioisotope. *Physica B: Condensed Matter*. 2021. **607**. P. 412850. https://doi.org/10.1016/j.physb.2021.412850.
6. Slight T.J., Yadav A., Odedina O. *et al.* InGaN/GaN laser diodes with high order notched gratings. *IEEE Photonics Technol. Lett*. 2017. **29**. P. 2020–2022. https://doi.org/10.1109/LPT.2017.2759903.
7. Ruhnke N., Müller A., Eppich B. *et al.* Compact deep UV system at 222.5 nm based on frequency doubling of GaN laser diode emission. *IEEE Photonics Technol. Lett*. 2018, **30**. P. 289–292. https://doi.org/10.1109/LPT.2017.2787463.
8. Anwar A.R., Usman M., Munsif M., Saba K. Reduction of efficiency droop by inserting superlattice quaternary-ternary electron blocking layer in GaN-based light-emitting diodes. *Mater. Sci. Eng.: B*. 2021. **271**. P. 115279. https://doi.org/10.1016/j.mseb.2021.115279.

9. Tang X., Ma Z., Han L. *et al.* Stripping GaN/InGaN epitaxial films and fabricating vertical GaN-based light-emitting diodes. *Vacuum*. 2021. **187**. P. 110160. https://doi.org/10.1016/j.vacuum.2021.110160.
10. Lee D.J., Ryu S.R., Kumar G.M. *et al.* Piezo-phototronic effect triggered flexible UV photodetectors based on ZnO nanosheets/GaN nanorods arrays. *Appl. Surf. Sci*. 2021. **558**. P. 149896. https://doi.org/10.1016/j.apsusc.2021.149896.
11. Chen Y., Wu Y., Ben J. *et al.* A high-response ultraviolet photodetector by integrating GaN nanoparticles with graphene. *J. Alloys Compnd*. 2021. **868**. P. 159281. https://doi.org/10.1016/j.jallcom.2021.159281.
12. Bouzid F., Pezzimenti F., Dehimi L. *et al.* Numerical simulations of the electrical transport characteristics of a Pt/*n*-GaN Schottky diode. *Jpn. J. Appl. Phys*. 2017. **56**. P. 094301. https://doi.org/10.7567/JJAP.56.094301.
13. Bouzid F., Dehimi L., Pezzimenti F. Performance analysis of a Pt/*n*-GaN Schottky barrier UV detector. *J. Electron. Mater.* 2017. **46**. P. 6563–6570. https://doi.org/10.1007/s11664-017-5696-1.
14. Bouzid F., Dehimi L., Pezzimenti F., Hadjab M., Larbi A.H. Numerical simulation study of a high efficient AlGaN-based ultraviolet photodetector. *Superlattices Microstruct*. 2018. **122**. P. 57–73. https://doi.org/10.1016/j.spmi.2018.08.022.
15. Lv Z., Liu L., Sun Y. *et al*. Absorption enhancement of ultraviolet detector in plasmonic nanoparticles-decorated GaN/AlGaN nanostructures. *Opt. Commun*. 2021. **492**. P. 126972. https://doi.org/10.1016/j.optcom.2021.126972.
16. Yakimov E.B., Polyakov A.Y., Shchemerov I.V. *et al.* On the nature of photosensitivity gain in Ga_2O_3 Schottky diode detectors: Effects of hole trapping by deep acceptors. *J. Alloys Compd*. 2021. **879**. P. 160394. https://doi.org/10.1016/j.jallcom.2021.160394.
17. Upadhyay K.T., Chattopadhyay M.K. Sensor applications based on AlGaN/GaN heterostructures. *Mater. Sci. Eng.: B*. 2021. **263**. P. 114849. https://doi.org/10.1016/j.mseb.2020.114849.
18. Chen Q., Yang J.W., Osinsky A. *et al.* Schottky barrier detectors on GaN for visible–blind ultraviolet detection. *Appl. Phys. Lett*. 1997. **70**. P. 2277. https://doi.org/10.1063/1.118837.
19. Zhao D.G., Jiang D.S. *GaN Based Ultraviolet Photodetectors, Photodiodes – World Activities in 2011* (Prof. Jeong Woo Park (Ed.). InTech., 2011.
20. Zhang S., Zhao D.G., Jiang D.S. *et al.* Investigation of responsivity decreasing with rising bias voltage in a GaN Schottky barrier photodetector. *Semicond. Sci. Technol*. 2008. **23**. P. 105015. https://doi.org/10.1088/0268-1242/23/10/105015.
21. Mou W., Zhao L., Chen L. *et al.* GaN-based Schottky barrier ultraviolet photodetectors with graded doping on patterned sapphire substrates. *Solid-State Electronics*. 2017. **133**. P. 78. https://doi.org/10.1016/j.sse.2017.04.008.
22. Sun X., Li D., Li Z. *et al.* High spectral response of self-driven GaN-based detectors by controlling the contact barrier height. *Sci. Rep.* 2015. **5**. P. 16819. https://doi.org/10.1038/srep16819.
23. Teisseyre H., Perlin P., Suski T. *et al.* Temperature dependence of the energy gap in GaN bulk single crystals and epitaxial layer. *J. Appl. Phys*. 1994. **76**. P. 2429. https://doi.org/10.1063/1.357592.
24. Baik K.H., Irokawa Y., Ren F., Pearton S.J., Park S.S. Temperature dependence of forward current characteristics of GaN junction and Schottky rectifiers. *Solid-State Electron.* 2003. **47**. P. 1533. https://doi.org/10.1016/S0038-1101(03)00071-6.
25. Pearton S.J., Abernathy C.R., Ren F. *Gallium Nitride Processing for Electronics, Sensors and Spintronics*. London, Springer, 2006.
26. Shockley W., Read W.T. Statistics of the recombinetions of holes and electrons. *Phys. Rev.* 1952. **87**. P. 835. https://doi.org/10.1103/PhysRev.87.835.
27. *Silvaco Atlas User's Manual*, Device Simulator Software, 2013.
28. Razeghi M., Henini M. *Optoelectronic Devices: III-Nitrides*, Amsterdam, Elsevier, 2004.
29. Caughey D., Thomas R. Carrier mobilities in silicon empirically related to doping and field. *Proc. IEEE*. 1967. **55**. P. 2192. https://doi.org/10.1109/proc.1967.6123.
30. Mnatsakanov T.T., Levinshtein M.E., Pomortseva L.I. *et al.* Carrier mobility model for GaN. *Solid-State Electron*. 2003. **47**. P. 111. https://doi.org/10.1016/S0038-1101(02)00256-3.
31. Canali C., Majni G., Minder R., Ottaviani G. Electron and hole drift velocity measurements in silicon and their empirical relation to electric field and temperature. *IEEE Trans. Electron Devices*. 1975. **22**. P. 1045–1047. https://doi.org/10.1109/T-ED.1975.18267.
32. Rhoderick E.H., Williams R.H. *Metal-Semiconductor Contacts*. Oxford, Clarendon Press, 1988.
33. Henisch H.K. *Semiconductor Contacts*. London, Oxford University, 1984.
34. Schmitz A.C., Ping A.T., Khan M.A. *et al*. Schottky barrier properties of various metals on *n*-type GaN. *Semicond. Sci. Technol*. 1996. **11**. P. 1464. https://doi.org/10.1088/0268-1242/11/10/002.
35. Monroy E., Calle F., Muñoz E. *et al*. $Al_xGa_{1-x}N$:Si Schottky barrier photodiodes with fast response and high detectivity. *Appl. Phys. Lett*. 1998. **73**. P. 2146. https://doi.org/10.1063/1.122405.

Authors' contributions

Fayçal Bouzid: conceptualization, methodology, formal analysis, investigation, data curation, writing – original draft, writing – review & editing, visualization.

Fortunato Pezzimenti: validation, investigation, writing – review & editing.

Authors and CV

Fayçal Bouzid received the PhD degree in materials physics from the University of Biskra, Algeria, in 2018. He is currently a senior researcher in the structures and devices division of the Research Center in Industrial Technologies CRTI-Algeria. He is involved in photovoltaics, thermophoto-voltaics, nuclear micro-batteries, and wide-gap semiconductor device modeling for UV photodetectors and laser sources.
https://orcid.org/0000-0002-2237-4789

Fortunato Pezzimenti received the Laurea and PhD degrees in electronic engineering from the Mediterranea University of Reggio Calabria, Reggio Calabria, Italy, in 2000 and 2004, respectively. Since 2006, he has been an Assistant Professor of electronics at the Mediterranea University of Reggio Calabria. His current research interests include design, modeling, and electrical characterization of wide bandgap semiconductor devices for high-power, high-frequency, and high-temperature applications.
E-mail: fortunato.pezzimenti@unirc.it;
https://orcid.org/0000-0002-8410-0142

Вплив товщини фронтального металевого шару платини в ультрафіолетових фотоприймачах Шотткі на основі GaN

F. Bouzid, F. Pezzimenti

Анотація. У цій роботі оцінено вплив товщини фронтального металевого шару на електрооптичні характеристики ультрафіолетового (УФ) детектора з бар'єром Шотткі на основі нітриду галію *n*-типу (*n*-GaN) за допомогою точного моделювання приладу та чисельного моделювання. Після порівняння вольт-амперних характеристик $J(V)$, розрахованих з використанням різних металів, було виявлено, що найбільш придатним металом для формування контакта Шотткі є платина (Pt). Отримані результати показують, що товщина фронтального платинового контакта Шотткі сильно впливає на спектральну чутливість детектора в розглянутому УФ-діапазоні 0,2…0,4 мкм. Зокрема, при кімнатній температурі чутливість детектора може досягати пікового значення 0,208 $A \cdot W^{-1}$ для довжини хвилі 0,364 мкм і напівпрозорого шару Pt товщиною всього 1 нм. Потім воно поступово зменшується зі збільшенням товщини металевого шару до 0,147 $A \cdot W^{-1}$ для Pt товщини 100 нм.

Ключові слова: нітрид галію, бар'єр Шотткі, ультрафіолетовий детектор, фотострум, чутливість.